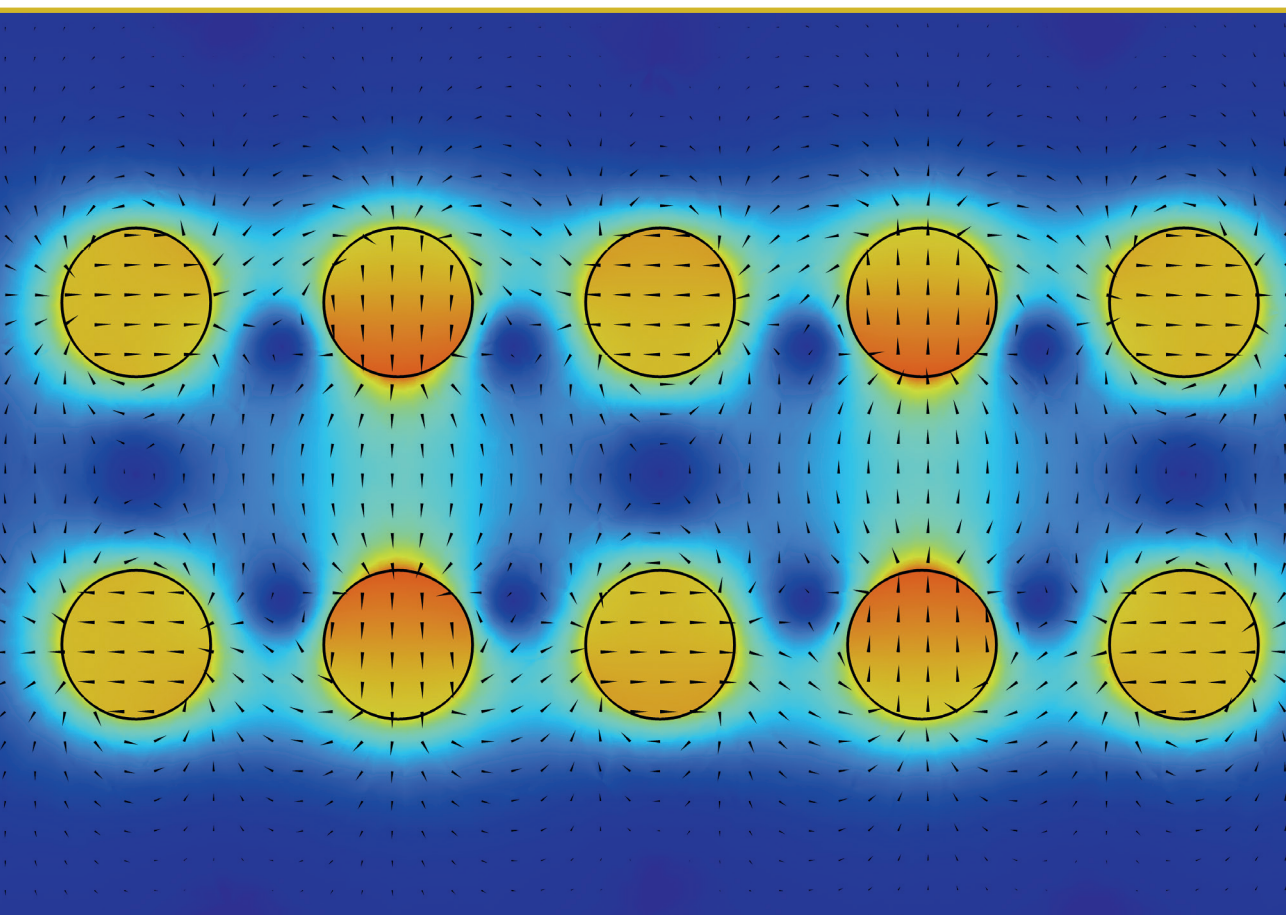


**Matīss Kalvāns**

**DYNAMIC ANALYSIS AND OPTIMIZATION  
OF ROTATING PERMANENT MAGNET  
DIPOLE PUMPS FOR METALLURGY**

Summary of the Doctoral Thesis



**RIGA TECHNICAL UNIVERSITY**

Faculty of Mechanical Engineering, Transport and Aeronautics  
Institute of Mechanics and Mechanical Engineering

**Matīss Kalvāns**

Doctoral Student of the Study Programme “Engineering Technology, Mechanics and  
Mechanical Engineering”

**DYNAMIC ANALYSIS AND OPTIMIZATION  
OF ROTATING PERMANENT MAGNET DIPOLE  
PUMPS FOR METALLURGY**

**Summary of the Doctoral Thesis**

Scientific supervisors

Professor Dr. sc. ing.  
JĀNIS AUZIŅŠ

Dr. phys.  
ANDRIS BOJAREVIČS

RTU Press  
Riga 2023

Kalvāns, M. Dynamic Analysis and Optimization of Rotating Permanent Magnet Dipole Pumps for Metallurgy. Summary of the Doctoral Thesis. Riga: RTU Press, 2023. – 31 p.

Published in accordance with the decision of the Promotion Council “P-04” of 2 June 2023, Minutes No. 56.

Cover picture by Matīss Kalvāns

<https://doi.org/10.7250/9789934229602>  
ISBN 978-9934-22-960-2 (pdf)

# **DOCTORAL THESIS PROPOSED TO RIGA TECHNICAL UNIVERSITY FOR THE PROMOTION TO THE SCIENTIFIC DEGREE OF DOCTOR OF SCIENCE**

To be granted the scientific degree of Doctor of Science (Ph. D.), the present Doctoral Thesis has been submitted for the defence at the open meeting of RTU Promotion Council on 20 September, 2023, 14.30 at the Faculty of Mechanical Engineering, Transport and Aeronautics Faculty of Riga Technical University, 6b, Ķīpsalas Street, Room 521.

## **OFFICIAL REVIEWERS**

Professor Dr. sc. ing. Andrejs Krasņikovs  
Riga Technical University

Professor Dr. phys. Andris Jakovičs  
University of Latvia, Latvia

Professor Dr.-Ing. Egbert Baake  
Leibniz Universität Hannover, Germany

## **DECLARATION OF ACADEMIC INTEGRITY**

I hereby declare that the Doctoral Thesis submitted for review to Riga Technical University for promotion to the scientific degree of Doctor of Science (Ph. D.) is my own. I confirm that this Doctoral Thesis has not been submitted to any other university for promotion to a scientific degree.

Name, surname ..... (signature)

Date: .....

The Doctoral Thesis has been written in Latvian. It consists of an introduction, 4 chapters, conclusions, 98 figures, 5 tables, 1 appendix; the total number of pages is 101, including appendices. The Bibliography contains 83 titles.

## CONTENTS

TOPICALITY.....	5
AIM OF THE THESIS.....	5
SCIENTIFIC NOVELTY.....	5
PUBLICATIONS.....	6
1. SINGLE PERMANENT MAGNET DIPOLE PUMPS .....	8
1.1. Single PM cylinder model pump.....	8
1.2. Numerical modelling of a single cylinder PM dipole pump.....	11
1.3. Investigation of single PM pump liquid metal flow in a linear channel.....	15
1.4. Industrial prototype .....	18
2. MULTIPLE PERMANENT MAGNET PUMPS .....	21
2.1. Double-sided pump .....	21
3. LIQUID METAL MIXERS .....	24
3.1. Model experiment for temperature homogenisation of molten metal with a rotating permanent magnet .....	24
3.2. Two-cylinder mixer .....	28
4. CONCLUSIONS .....	30
BIBLIOGRAPHY .....	31

## **TOPICALITY**

Liquid metal pumps are mainly used in nuclear reactors and metallurgy. Electromagnetic induction pumps using current windings are already widely known, but permanent magnet devices have been relatively little studied. With the development of rare earth permanent magnets, electromagnetic induction pumps using permanent magnets have become increasingly available for a variety of applications.

## **AIM OF THE THESIS**

The aim of the Doctoral Thesis is to investigate liquid metal pumps with rotating cylindrical magnets whose magnetization is perpendicular to their axis of symmetry and to assess the application of such equipment to metallurgical processes. Within this goal, a new type of electromagnetic devices for metallurgical applications using rotating dipoles of permanent magnets is proposed.

To achieve the set goal, the following tasks were set:

- to perform research and analysis of existing permanent magnet pumps for metallurgical applications;
- to study the materials of permanent magnets and their applications in metallurgy;
- to perform theoretical calculations of parameters of pumps with rotating permanent magnets;
- to perform an experimental study of the electromagnetic parameters of pumps with permanent magnets and the generated liquid metal flows;
- to find rational and optimal parameters of pumps with permanent magnets for metallurgical applications;
- to develop numerical models for the calculation of pump parameters and to perform their verification and validation.

## **THESES**

- In the liquid metal pump, in which the cylinders of permanent magnets are located in two rows, there is an optimal arrangement of magnetization directions of mutual permanent magnets, which ensures stable operation of the device.
- Permanent magnet pumps can be used for metallurgical tasks such as mixing, pumping, velocity measurement, degassing, as well as hydrostatic pressure generation.

## **SCIENTIFIC NOVELTY**

The Thesis investigates various MHD machines that utilize permanent magnets for metallurgical applications. The proposed MHD devices incorporate rotating, radially magnetized permanent magnets. The MHD device developed in this study with multiple permanent magnets offers a novel technical solution that has not been previously reported in the literature. An optimization problem was solved to determine the best arrangement of magnets for designing such a device, ensuring optimal operation. These MHD systems have demonstrated high efficiency, making them ideal for use in metallurgical furnaces to aid in mixing and delivering molten metal from the furnace to the crystalliser.

## PUBLICATIONS

The main results of the Thesis are presented in 12 scientific publications in journals and peer-reviewed conference proceedings.

Publications indexed in SCOPUS and Web of Science databases:

1. **Kalvāns, M.**, Bojarevičs, A., Beinerts, T., & Gaile, A. (2022). Single Dipole Permanent Magnet Induction Pump for Liquid Metals. *Magnetohydrodynamics (0024-998X)*, 58.
2. Berga, K. K., Berenis, D., **Kalvāns, M.**, Krastiņš, I., Beinerts, T., Grants, I., & Bojarevičs, A. (2022). Model Experiment for Molten Metal Temperature Homogenization with Rotating Permanent Magnet. *JOM*, 74(6), 2450–2460.
3. **Kalvāns, M.**, & Bojarevičs, A. (2020). Bilateral Liquid Metal Pump with Permanent Magnets. *Magnetohydrodynamics (0024–998X)*, 56(1).
4. Kaldre, I., Bojarevičs, A., Beinerts, T., Baranovskis, R., Nikoluskins, R., Milgrāvis, M., & **Kalvāns, M.** (October 2018). Contactless electromagnetic method for aluminium degassing. In: *IOP Conference Series: Materials Science and Engineering (Vol. 424, No. 1, p. 012057)*. IOP Publishing.

Patents:

5. Bojarevičs, J. Geļfgats, T. Beinerts, **M. Kalvāns**, and R. Baranovskis, “Elektrovadošu metālisku un pusvadītāju kausējumu maisīšanas ierīce,” LV15144, 2016.

Publications in conference proceedings and journals:

6. Bojarevičs, R. Baranovskis, T. Beinerts, and **M. Kalvāns**, “Two Cylinder Permanent Magnet Liquid Metal Stirrer”, in *Proceedings of the 10th PAMIR International Conference “Fundamental and Applied MHD,” 2016*, pp. 431–435.
7. **Kalvāns, M.**, Bojarevičs, A., Kaldre, I., and Beinerts, T. “Assessment of Linear Permanent Magnet Liquid Metal Dispenser”, in *Proceedings of the 10th PAMIR International Conference “Fundamental and Applied MHD,” 2016*, pp. 289–293.

Participation in international scientific conferences:

8. **Kalvāns, M.**, Berga, K. K., Berenis, D. et al. “Model Experiment for Aluminum Melt Temperature Mixing with Rotating Permanent Magnets”, 4th Conference & Exhibition on Light Materials, 2–4 November 2021, virtual conference.
9. **Kalvāns, M.**, Bojarevičs, A. “One permanent magnet dipole induction pump for liquid metals”, meeting of the UL 79th conference section “Electromagnetic processing and research methods of materials”, February 26, 2021, Riga, Latvia.
10. **Kalvāns, M.**, Bojarevičs, A., and Beinerts, T. “Linear Permanent Magnet Liquid Metal Pump,” in 11th PAMIR International Conference – Fundamental and Applied MHD, 2019, pp. 312–316.

11. **Kalvāns, M.**, Bojarevičs, A., Beinerts, T. “Ten permanent magnet bilateral pump”, meeting of the UL conference section “Electromagnetic processing and research methods of materials” February 9, 2018, Riga, Latvia.
12. **Kalvāns, M.**, Bojarevičs, A. “Permanent Magnet Potential Difference Probe for 3D Liquid Metal Velocity Measurements”, 3rd International Workshop on Measuring Techniques for Liquid Metal Flows, April 13–18, 2015, Dresden, Germany.

# 1. SINGLE PERMANENT MAGNET DIPOLE PUMPS

## 1.1. Single PM cylinder model pump

Permanent magnet (PM) dipoles are known to produce higher magnetic field values than multipole PM systems at large distances from the PM surface [1]. This can be explained by the fact that in the case of multiple poles there is a decay of the magnetic field between the poles, which becomes significant as the distance increases. Considering that in industrial conditions the working substances have high temperatures and are contained in sealed containers with thick ceramic walls, the distances between the PM surface and the liquid metal are large, so the use of dipoles is suitable.

To demonstrate the efficiency of a liquid metal pump, a rotor consisting of a single dipole permanent magnet magnetized perpendicular to the axis of rotation is utilized. As the rotor rotates, it creates a traveling magnetic field within a narrow liquid metal channel. The resulting magnetic field induces an eddy electric field within the liquid metal. This, in turn, generates electric currents that interact with the original magnetic field, ultimately producing a force proportional to the square of the magnetic field induction intensity.

If a liquid metal channel is too thick, a backflow will form on the other side of the channel where the magnetic field is weaker. Therefore, an optimal channel thickness is required, neither too thin, creating additional hydrodynamic resistance, nor too thick. Similarly, the width of the channel must be considered, as it should be smaller than the length of the PM to maximise pump efficiency since the end effects of the PM reduce the magnetic field strength. The induced currents generated by the travelling magnetic field form concentric loops inside the liquid metal, with parallel currents along the side walls and the primary magnetic field. However, this results in a zero-vector product and no electromagnetic force, known as the edge effect, reducing the pump efficiency when the channel width is limited.

To investigate the potential use of a single rotating PM cylinder for pumping liquid metals, an experiment was conducted to transport liquid aluminium from the melting furnace and lift it higher. The results of this experiment are used to validate and adjust analytical calculations for single PM rotor induction pumps, specifically in the context of liquid metal transportation.

Certain physical similarity criteria must be met to apply these small-scale experimental results to an industrial-sized device. An experimental model was selected, 6 times smaller than the industrial-sized model due to practical constraints. Complete physical similarity is difficult to achieve, so only the most critical criteria were considered. The geometric similarity was evaluated with corresponding dimensionless quantities:

$$\frac{\tau}{h} = idem, \quad (1.1)$$

$$\frac{\tau}{W} = idem, \quad (1.2)$$

$$\frac{h}{R} = idem, \quad (1.3)$$

where  $\tau$  is the characteristic length, which is the distance over which the direction of the magnetic field changes by  $180^\circ$ ,  $h$  is the height of the channel,  $W$  is the width of the channel, and  $R$  is the radius of the magnet. Each of the parameters  $\tau$ ,  $h$ ,  $W$  and  $R$  is 6 times larger for the industrial model.

The most crucial aspect is achieving dynamic similarity, starting with dimensionless frequency. The notation 1 was used for the GaInSn model and the notation 2 for the aluminium model.  $\sigma$  is the electrical conductivity,  $\omega$  is the cyclic frequency,  $f$  is the rotational frequency, and  $\mu_0$  is the vacuum permeability constant.

$$\Omega_d = \sigma \cdot \omega \cdot \mu_0 \cdot \tau^2 = idem, \quad (1.4)$$

$$\sigma_1 \cdot \omega_1 \cdot \mu_0 \cdot \tau_1^2 = \sigma_2 \cdot \omega_2 \cdot \mu_0 \cdot \tau_2^2, \quad (1.5)$$

$$\omega = 2\pi f, \quad (1.6)$$

$$f_2 = \frac{\sigma_1}{\sigma_2} \cdot \frac{\tau_1^2}{\tau_2^2} f_1 = 0.023 f_1. \quad (1.7)$$

To achieve an equivalent hydrostatic pressure, the industrial model can use a 44 times lower PM rotation frequency, reducing the skin effect and improving the pump's efficiency. The next step was to evaluate the Stewart number, defined as the ratio of electromagnetic to inertial forces. The variables used in the equation are  $\rho$  for mass density and  $B$  for the PM remanent magnetic induction.

$$N = \frac{\sigma \cdot B^2 \cdot \tau}{\rho \cdot \omega \cdot \tau} = \frac{\sigma \cdot B^2}{\rho \cdot \omega} = idem, \quad (1.8)$$

$$B_2 = \sqrt{\frac{\sigma_1 \rho_1 \omega_1}{\sigma_2 \rho_2 \omega_2}} \cdot B_1 = 0.22 B_1 \quad (1.9)$$

To attain physical similarity, the larger model could use almost five times weaker magnets. Furthermore, the Hartmann number, defined as the ratio of electromagnetic to viscous forces, was also evaluated.

$$Ha = B \cdot \tau \cdot \sqrt{\frac{\sigma}{\nu}}, \quad (1.10)$$

where  $\sigma$  is the electrical conductivity and  $\nu$  is the kinematic viscosity. In Table 1.1, the most important parameters between the GaInSn and the aluminium model are compared.

Table 1.1

Comparison of Key Model Parameters

	$\rho$ , kg/m <sup>3</sup>	$\sigma$ , S/m	$\tau$ , mm	$h$ , mm	$W$ , mm	$R$ , mm	$L$ , mm	$f$ , Hz
GaInSn	6360	$3.3 \times 10^6$	52	7	73	25	100	71
Aluminium	2400	$4 \times 10^6$	312	42	438	150	600	1,6

The experimental device comprises a single NdFeB PM cylinder magnet that is magnetised perpendicular to its rotation axis, with a magnetisation of  $B = 1.4$  T. Figure 1.1 shows a schematic of the magnet and channel. The magnet has a diameter of 50 mm and a length of 100 mm. Along

its entire length, the magnet has grooves that are 4 mm wide and 4 mm deep. These grooves have minimal impact on the magnetic field generated by the PM cylinder. Metal rods were inserted into the grooves and attached to the outer casing to prevent rotation between the magnet and its frame. The grooves are perpendicular to the magnetic poles to minimise the loss of magnetic field intensity, which would otherwise be greater in a different position.

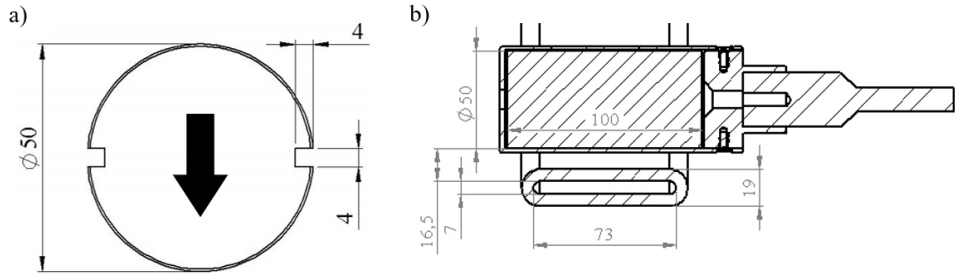


Fig. 1.1. a) Cross-section of the permanent magnet; b) cross-section of the flattened rubber tube with the PM rotor.

Figure 1.2 shows the hydrostatic pressure values obtained from experimental measurements and numerical calculations. The numerical model determined the maximum pressure at the middle of the side face. However, it is important to note that the numerical model considered a smaller volume than the electromagnetic interaction, which may have resulted in the experimental data showing higher pressure values.

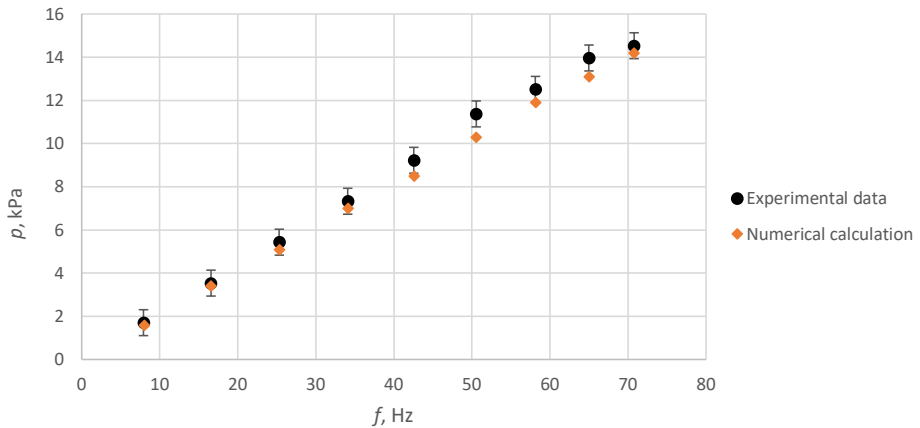


Fig. 1.2. Hydrostatic pressure of liquid metal depending on the frequency of rotation.

Based on the results obtained, it can be concluded that a single PM cylinder can efficiently pump liquid metal when positioned near a narrow channel. The rotation of the PM induces heating in the liquid metal, which, in turn, reduces its conductivity. This heating effect is desirable in practical applications, as it is often necessary in metallurgy.

## 1.2. Numerical modelling of a single-cylinder PM dipole pump

A numerical model was developed to predict the performance of the liquid metal pump discussed in the previous chapter under different parameters. The model was created using the *Comsol Multiphysics* program and involved a rotating permanent magnet near a liquid metal region. The model investigated the parameters of the pump at various channel sizes while keeping the rotation speed of the magnet constant at 25 Hz. The geometric model comprised an air cube with a side of 0.3 m, a channel, and a permanent magnet. The channel was filled with liquid aluminium, so its properties are as follows – relative permeability  $\mu_r = 1$ ; electrical conductivity  $\sigma = 3.46 \times 10^6$ ; density  $\rho = 6440 \text{ kg/m}^3$ ; dynamic viscosity  $\mu = 2.4 \times 10^{-3}$ . The fluid was assumed incompressible, and the turbulence model type was selected as RANS. A no-slip boundary condition was set for the channel's side walls. Under the turbulent flow packet, the volume force was chosen as  $\text{mf.FLTxx}$ ,  $\text{mf.FLTyy}$ ,  $\text{mf.FLTzz}$  at x, y and z coordinates to read the calculated electromagnetic force from magnetic field packets. A speed of  $-2 \text{ m/s}$  was initially set for the y-axis to establish a stationary mode more quickly, and a pressure of 0 Pa was selected as the boundary condition at the entrance plane of the channel. A pressure of 1 Pa was chosen as the boundary condition at the exit plane of the channel because the model did not work when 0 Pa was chosen. The finite element mesh was created using free tetrahedral triangles, with a coarse maximum element size of 0.057 m for the airspace region, and a normal maximum element size of 0.057 m for the magnet region. The fluid region had an extremely fine grid element size, with a manually modified maximum element size of 0.035 m. A stationary model was solved initially, and the results were then fed into the time-varying model, which solved the model up to a duration of 2 s.

Using the above-described model, the flow rate was analysed in relation to the dimensions of the channel. Specifically, the width of the channel was varied while keeping the distance from the magnet to the nearest channel edge constant. Figure 1.3 shows the flow rate in a channel with a height of 7 mm and a width of 70 mm, while Fig. 1.4 shows the flow rate in a channel with a height of 17 mm and a width of 170 mm.

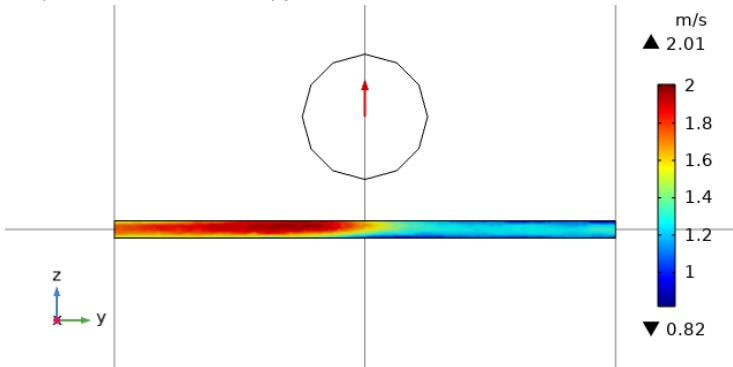


Fig. 1.3. Liquid metal flow rate at the z/y plane slice in the mid-plane of the channel. Channel height 7 mm, width 70 mm.

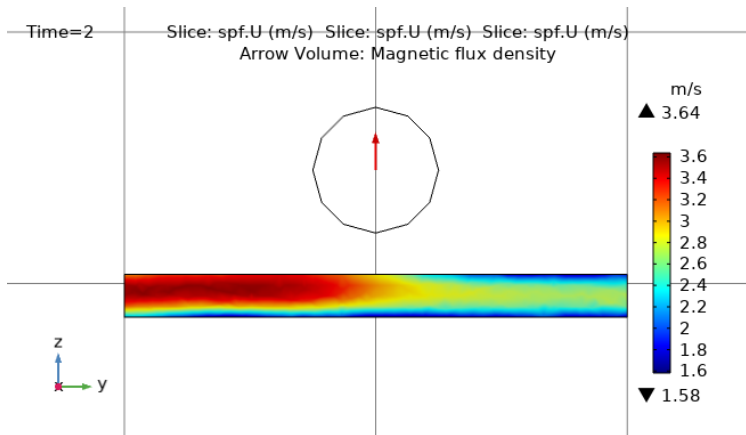


Fig. 1.4. Liquid metal flow rate at the z/y plane slice in the mid-plane of the channel. Channel height 17 mm, width 170 mm.

Table 1.1

Calculated Flow Rate for Each Channel Size

Flow rate (L/s)		Channel height (mm)		
		7	12	17
Channel width (mm)	70	<b>0.83</b>	<b>1.83</b>	<b>2.90</b>
	120	<b>1.71</b>	<b>3.85</b>	<b>6.16</b>
	170	<b>2.22</b>	<b>5.17</b>	<b>8.4</b>

Taking these 9 points into account, an optimisation task was created, resulting in the response surface shown in Fig 1.5.

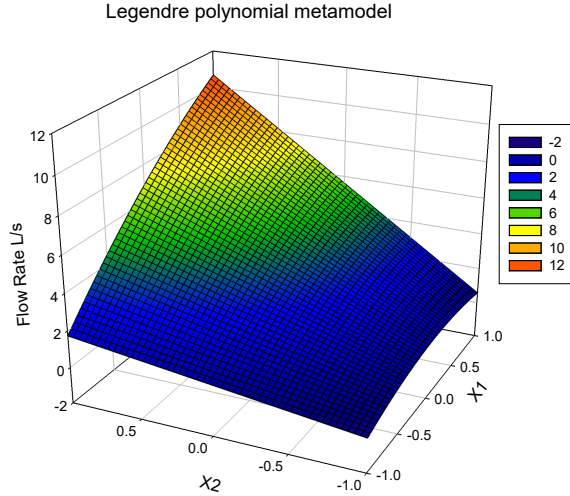


Fig 1.5. Legendre polynomial metamodel.

A second-order regression model was used for approximation, which provided 11.1 % relative cross-validation error and  $R^2 = 0.998$ . This model can help to create an optimal channel design, because it shows what factors should be to get the optimal response value. In this case, the model does not provide significant information as it shows that larger channel sizes will result in higher throughput. The response surface can be expressed as a 2nd-order polynomial:

$$F = -1.35333 + 0.01822x_1 - 0.06987x_2 - 0.00014x_1^2 - 0.00411x_1x_2 \quad (1.11)$$

To simulate the situation in which the pump must lift the liquid metal to a higher tank, the numerical model introduced a higher back pressure at the outlet of the channel. Specifically, a back pressure of  $p = 4000$  Pa was chosen. As shown in Fig. 1.6, under these conditions, the flow takes on a recirculating pattern in which the metal on the side of the channel flows back against the main stream. Figure 1.6 represents a slice of the  $x/y$  plane, while Fig. 1.7 shows a slice of the  $z/x$  plane, and Fig. 1.8 depicts a slice of the  $z/y$  plane. The maximum flow velocity, at 0.87 m/s, is achieved in the central part of the channel.

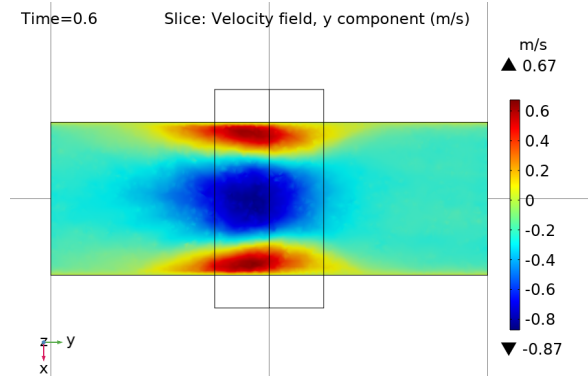


Fig. 1.6. Liquid metal flow rate in the x/y plane slice in the mid-plane of the channel.

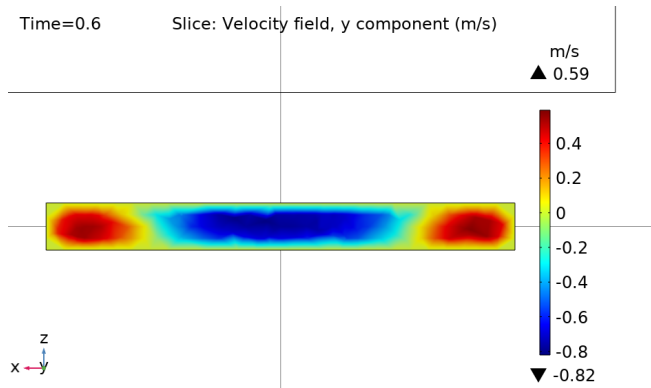


Fig. 1.7. Liquid metal flow rate in the z/x plane slice in the mid-plane of the channel.

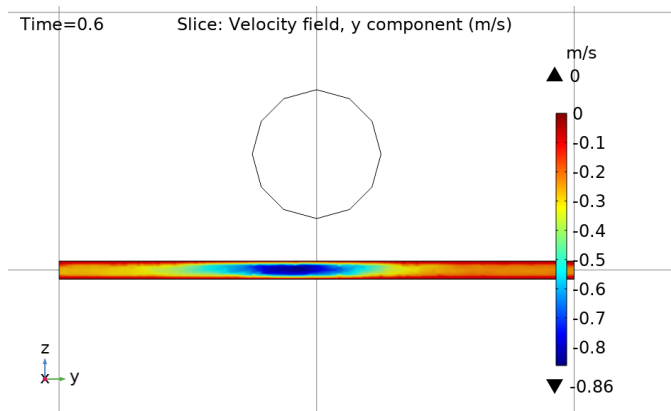


Fig. 1.8. Liquid metal flow rate in the z/y plane slice in the mid-plane of the channel.

By performing calculations at different pressure values, the characteristic curve  $Q$  of  $p$  was obtained, which is an important parameter for any pump (see Fig. 1.9).

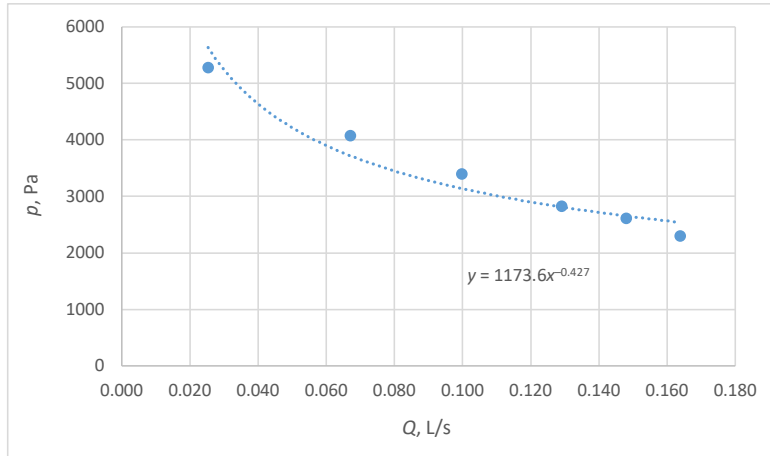


Fig. 1.9. Characteristic curve  $Q$  of pump  $p$ .

### 1.3. Investigation of single PM pump liquid metal flow in a linear channel

This chapter investigates the liquid metal flow in a rectangular channel generated by a permanent magnet pump. Liquid metal flow has several applications in metallurgical processes. Firstly, when the channel's ends are open, it can transport liquid metal from one production phase to another. Secondly, it can disperse and homogenise added particles in the melt. In producing metal matrix composites (MMCs), nanoparticles tend to form large agglomerates that are difficult to disperse. By introducing a high-intensity turbulent flow of liquid metal, sufficient shear force can be generated to disperse the agglomerates and distribute them uniformly throughout the melt volume. This intense melt flow can be achieved by closing both ends of the channel and allowing it to act as a sealed vessel. Thirdly, it can be used for the non-contact melt degassing process. Closing both ends of the channel provides a highly turbulent flow that could effectively disperse inert gas bubbles and degass the melt. Aluminium degassing is necessary to remove hydrogen dissolved in the melt [2].

Hydrogen is the most soluble gas in aluminium, and its solubility in liquid aluminium is one order of magnitude higher than in solid aluminium. As a result, hydrogen pores are formed during melt crystallisation, reducing the mechanical strength of the final material [3].

The most common way to reduce the hydrogen concentration in aluminium is to introduce an inert gas, such as argon, into the melt, into which the dissolved hydrogen can diffuse. This diffusion causes hydrogen to migrate into the bubbles with zero hydrogen concentration, which is then expelled from the melt volume through its surface by the Archimedean force. When hydrogen leaves the melt, it burns in contact with oxygen. Due to the high surface tension of the metal, argon bubbles are formed with a low surface area to volume ratio, so a large amount of inert gas is required for melt degassing [4]. An experimental model was designed to measure pressure, flow velocity, and flow structure in a rectangular channel. The experimental prototype was designed as

a closed circuit due to the limited amount of metal available for the experiment and to reduce the probability of leakage and metal oxidation. Figure 1.10 shows a picture of the experimental system, divided into the active and peripheral parts of the channel.

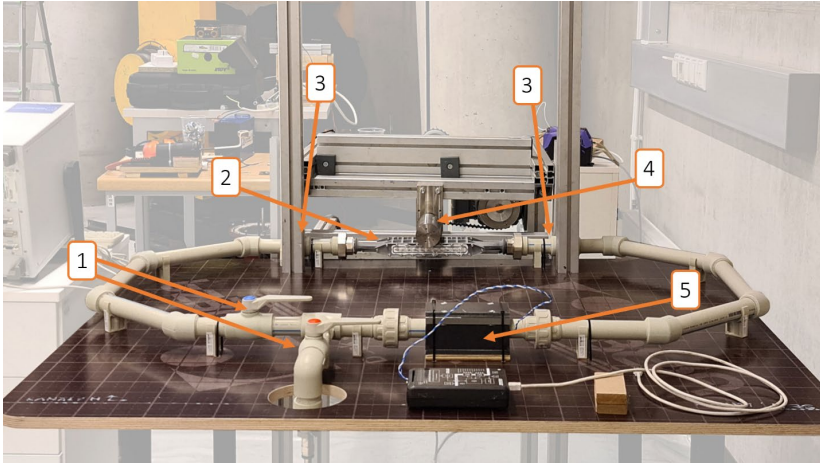


Fig. 1.10. Experimental model: 1 – valve; 2 – 3D printed linear part; 3 – manometer location; 4 – permanent magnet rotor; 5 – flow meter; the squares on the table correspond to 10 cm×10 cm.

The system's central component consists of a 3D-printed part with a rectangular volume inside. An atmospheric manometer is positioned 100 mm from the sides of the rectangular channel to measure pressure drop in the pumping region.

The permanent magnet rotor device comprises a cylindrical permanent magnet, a shaft, gears, a timing belt, a three-phase motor, a frequency converter, and aluminium profiles for adjusting the magnet's position. To prevent the transfer of large vibrations, the rotor and its drive mechanism are not connected to the table on which the liquid metal channel is located.

The rotor is a cylindrical dipole with a diameter of 50 mm and a height of 100 mm. The remanent magnetisation  $B$  is 1.4 T and is directed perpendicular to the cylinder's axis. The PM rotor contains a single NdFeB magnet in a 1 mm thick stainless steel shell. The magnet was placed in the bend of the linear channel wall to reduce the distance between the magnet and the liquid metal. The non-magnetic distance is approximately 5.2 mm. The rotor's axis coincides with the midpoint of the linear part of the channel. A small oscillation of the magnet rotation, with an amplitude of less than 0.2 mm, was observed at magnet rotation speeds up to 25 Hz. At higher speeds, the rotor's oscillations decreased, but the mechanical vibrations of the overall device increased. Due to the device's design, the rotor can operate at speeds between 5 and 50 Hz, when the mechanical vibrations of the machine begin to compromise the precise positioning of the magnet near the channel.

The peripheral part of the system was made of PPR fusible pipes and joints with an inner diameter  $D_p = 23$  mm to ensure channel strength and hermeticity, as well as chemical inertness and ease of assembly. The duct includes valves for flow control, a metal inlet and outlet, and a conduction flow meter. The channel's total volume is approximately 1.5 L. The channel was filled

using a specially designed stainless-steel container, from which the metal was forced out with the help of argon to provide a certain volume in the channel while protecting the metal from contact with air.

The experimental system can be used in two types of experiments: by closing the valve and reducing the flow in the peripheral part of the channel, a degassing channel or tank is simulated; while with the valve open and maximum flow, metal pumping through the channel can be simulated.

The internal cross-section of the central part is rectangular with a height of  $b$ , a width of  $2a$ , and a length of  $l$ , as shown in Fig. 1.11. 3D printing was used for the central channel component to obtain the desired shape. This experiment was preceded by tests that led to the selection of PA12 material. To ensure velocity measurements with the PUDV method through the sides, a 6 mm thick plexiglass part with cylindrical holes was created so that the ultrasonic manometers could be accurately positioned. The 3D-printed part with plexiglass edges and a gasket is visible in Fig. 1.11. This design facilitates the measurement of the liquid metal flow rate, is hermetic and rigid, and is composed of a chemically inert material that does not react with GaInSn. The material is also non-conductive, simulating ceramic walls under industrial conditions.

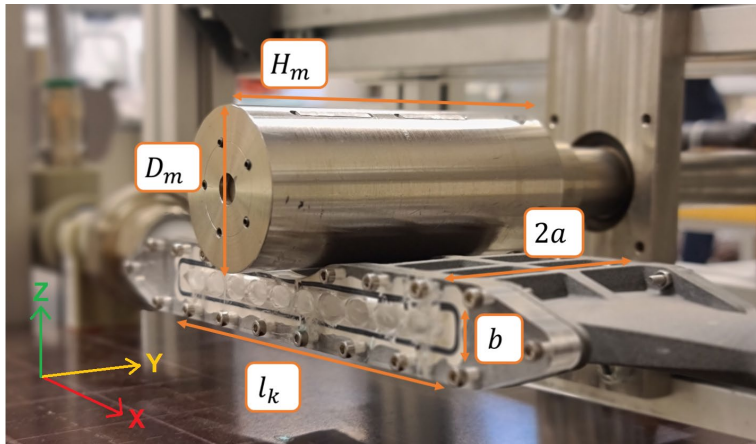


Fig. 1.11. A close-up of the linear part of the experimental apparatus, denoting the position of the permanent magnet rotor and the linear channel, where  $H$  is the height of the rotor,  $D$  is the diameter of the rotor,  $2a$  is the width of the channel in the  $y$ -axis direction,  $b$  is the height of the channel in the  $z$ -axis direction, and  $l$  is the length of the linear part of the channel in the  $x$ -axis direction.

The device did not have active cooling, and to reduce the risk of leakage, there was no room for direct temperature measurements in contact with the liquid metal. Short series of experiments were performed, and the device was allowed to cool down between experiments. Although the volume of the channel can be considered closed, long series of experiments are not desirable, since the quality of velocity measurements deteriorates significantly in the case of prolonged and intense stirring. The situation was improved by purifying GaInSn by filtration and heating in an argon atmosphere, thereby getting rid of oxides and dissolved gases that had entered the metal from previous experiments.

Velocity measurements were made using a *Signal Processing* anemometer *DOP2000 v2125* using the pulsed ultrasound doppler velocity (PUDV) method. Only one probe was used for measurements at a time. The advantage of the method is information on the spatial distribution of speeds. Still, its disadvantage is the maximum or limited speed and the measured distance, which depends on the pulse repetition frequency  $f_{prf}$ , the sound speed in the medium  $c$  and the frequency of the transmitter  $f_c$ .

The valves are opened to simulate the EM pump and the maximum flow rate is obtained. The reconstructed velocity field for this mode is shown in Fig. 1.12 a. The measurements were taken from the  $y = 82$  mm side, and the results show that better data can be obtained closer to the opposite wall. At the wall, the velocity decreases but is not zero, which can be explained by the fact that the ultrasound beam has diverged and describes a larger volume than near the probe.

A unidirectional flow was obtained, flowing towards the x-axis with an average velocity  $v \sim 220$  mm/s and velocity pulsations  $v_{sd} = \pm 130$  mm/s, as seen in Fig. 1.12 b. At the wall, the speed decreases slightly but is not zero.

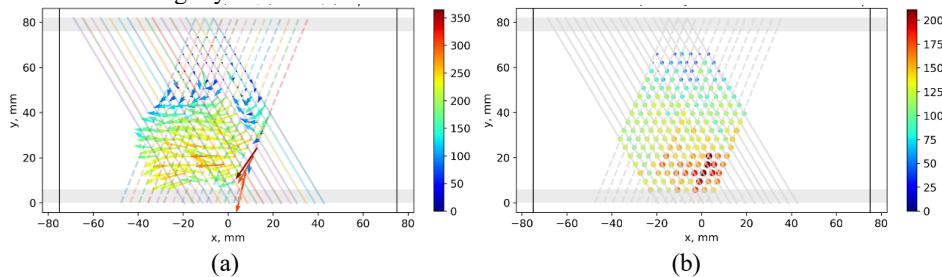


Fig. 1.12. (a) Reconstruction of the liquid metal flow field in EM pump mode; the grey horizontal area indicates plexiglass walls, the vertical lines delimit the linear part of the channel, the slanted lines indicate the ultrasound beam on which measurements are made both upstream and downstream; (b) standard deviation of velocity in EM pump mode.

Experimental measurements of velocity distribution can be challenging and sometimes yield low-quality data. Two main factors contribute to this. Firstly, GaInSn may produce impurities that lead to a weak UDV signal after prolonged intense mixing. Secondly, using only one UDV probe per experiment means combining results from multiple positions and angles is meaningful only if the flow pattern is consistent. However, inconsistencies between experimental measurements and numerical simulation results indicate that the flow pattern may be unpredictable and vary between experiments, even within a short interval of less than 30 seconds. One potential solution could be to conduct experimental measurements over a longer period of time so that long-term asymmetric patterns average closer to zero.

#### 1.4. Industrial prototype

An industrial prototype of a liquid metal pump was developed based on numerical models and experimental experience. The maximum size of permanent NdFeB magnets in the direction of magnetisation being 5 cm, larger magnets had to be assembled from smaller ones. To safely assemble such large magnets, various accessories were required to ensure operational safety, slow magnet convergence, and structural integrity of the magnet assembly. This pump was designed to

produce 40 t/h of liquid aluminium and lift the hydrostatic column to a height of 1.5 m. The magnet assembly in this device measures 70 cm in length and 15 cm in diameter.

To evaluate the device's performance, an experiment was conducted using an aluminium sheet. A  $10 \times 500 \times 1000$  mm aluminium sheet was placed directly under the rotor, and the force generated at different rotation speeds was measured. Figure 1.14 shows the measured force on the aluminium sheet. A photo of the device can be seen in Fig. 1.13.



Fig. 1.13. Photo from an experiment measuring the horizontal force on an aluminium sheet.

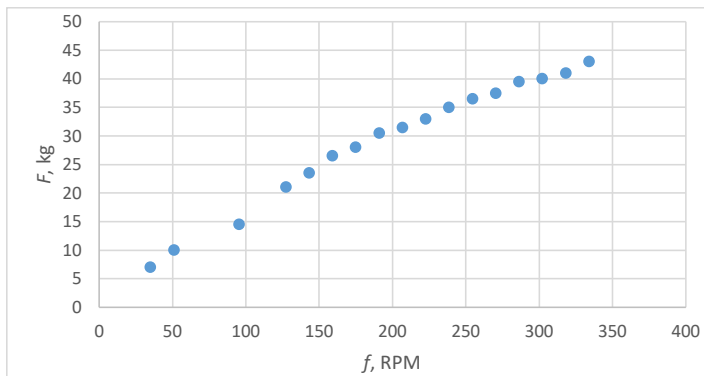


Fig. 1.14. Force on the sheet depending on the rotation speed of the magnet.

Furthermore, the motor's power consumption was measured as a function of the magnet's rotational speed (shown in Fig. 1.15).

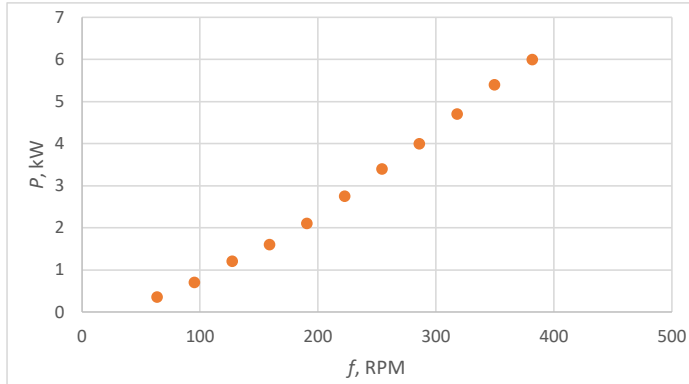


Fig. 1.15. The power consumed by the motor depends on the rotation speed of the magnet.

A test was also carried out with liquid aluminium under industrial conditions (Fig. 1.16). The pump was placed near a specially created rectangular channel, which then transitioned to a round tube that rises to a height of 1 m. In this test, the flow rate was estimated by measuring the amount of aluminium leached into a tank where the liquid level could be seen to rise. As a result, a productivity of 10 t/h was measured.



Fig. 1.16. Equipment test with liquid aluminium.

## 2. MULTIPLE PERMANENT MAGNET PUMPS

This chapter explores the potential of using multiple cylindrical PMs rotating synchronously to pump liquid metal. A Halbach assembly [5] is considered, in which the magnets are arranged in a single row such that the direction of the magnetic field changes by  $90^\circ$  for each successive magnet. This arrangement results in a stronger magnetic field on one side of the row of magnets than on the other, allowing for a smaller amount of magnetic material to achieve the necessary magnetic field strength. As permanent magnets are the costliest component of large PM pumps, this concept has the potential to offer significant benefits.

### 2.1. Double-sided pump

To achieve a high-performance liquid metal pump, a configuration is proposed where PM cylinders are positioned on both sides of a rectangular profile channel. Each side has a row of PMs with their rotation axis parallel to the channel walls and perpendicular to the liquid metal flow direction. The goal is to achieve the highest possible flow rate  $Q$  and pressure  $p$  simultaneously.

The experimental prototype's (Fig. 2.1) central part comprises two rows of cylindrical PM dipoles magnetised perpendicular to their rotation axis. Each magnet has a length of 200 mm and a diameter of 50 mm. The distance between two magnet axes in a row is 88 mm, and between magnet axes in opposite rows 115 mm. The angle  $\alpha$  represents the angle between the magnetisation of two consecutive magnets in the same row, and  $\beta$  is the angle between the first two magnets in opposite rows. Note that there may be a slight error when setting these angles in practice.

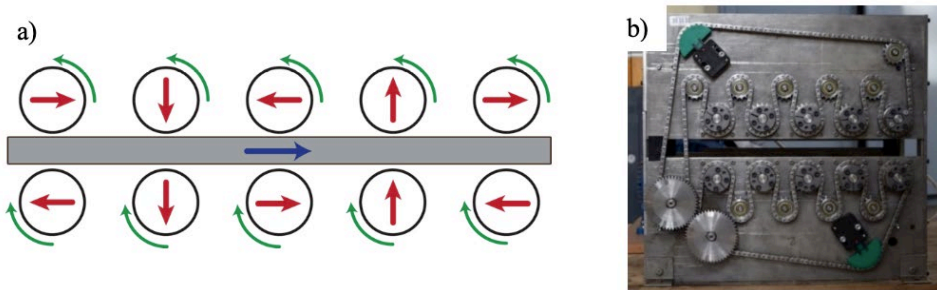


Fig. 2.1. a) Scheme of magnets ( $\alpha = 90^\circ$ ;  $\beta = 180^\circ$ ); b) experimental device.

The non-contact pumping of liquid metal is based on creating a travelling magnetic field. However, the interaction between two rotating magnetic dipoles can create a sinusoidal torque that places a heavy load on the mechanical drive, especially for large-scale pumps. Therefore, to ensure practical applications, a strong magnetic field with a small system torque is required. All PMs must rotate synchronously, with each row rotating in opposite directions, which can be achieved using gears, belts, or chains. However, the main drive unit must overcome the total torque. This chapter aims to determine the optimal configuration of PM magnetisation directions to achieve high PM rotational stability.

The study utilized steady-state and parametric 3D calculations in *COMSOL Multiphysics* (Fig. 2.2). A parametric analysis was conducted for angle  $\alpha$  and time  $t$ , with angle steps of  $1^\circ$  and time steps of 0.1 s. The magnetic field in the room was calculated to determine the force exerted on one of the PMs. The torque on each PM was calculated and summed to determine the system's resistance during one rotation. The model had 55547 elements and used a free tetrahedral finite element mesh.

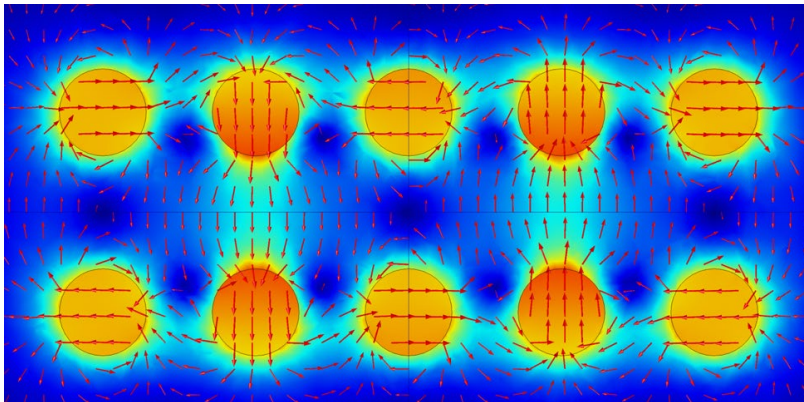


Fig. 2.2. Ten cylinders – amplitude and direction of magnetic field induction ( $\alpha = 90^\circ$ ;  $\beta = 180^\circ$ ).

The system with 10 cylinders exhibits three minima in the average torque  $T$  (Fig. 2.3). These minima occur at  $\alpha = 48^\circ$ , where  $T = 1.57 \text{ N} \cdot \text{m}$ ,  $\alpha = 93^\circ$ , where  $T = 0.59 \text{ N} \cdot \text{m}$ , and  $\alpha = 137^\circ$ , where  $T = 1.36 \text{ N} \cdot \text{m}$ . All three minima correspond to low torques, with the middle one being the lowest. The system with an angle  $\alpha = 93^\circ$  is the most efficient in terms of pumping efficiency and is also very similar to the Halbach arrangement, which creates a stronger magnetic field between the rows than outside.

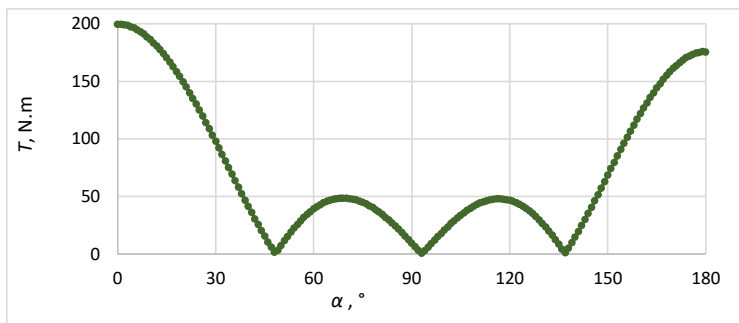


Fig. 2.3. Ten cylinders – system average torque ( $\beta = 180^\circ$ ).

In the case of 10 cylinders, the torque was measured experimentally using the values  $\alpha = 93^\circ$  and  $\beta = 180^\circ$ . The measurement was conducted to obtain the maximum value at full rotation

in both directions. The average measurement result was  $T = 18.7 \text{ N} \cdot \text{m}$ . Due to the inaccuracy of mutual angles and frictional forces, the experimental result is slightly higher than the theoretical calculation. It should be noted that measuring other phase shift angles was not possible because the torque values were too high and not permissible with the particular equipment. Furthermore, real systems of this type with more PM dipoles become increasingly impractical because, assuming a small phase shift angle error, the total shift is already significant when summing it up for all PM cylinders. A small shift from the optimal angle can dramatically increase the system's torque.

A series of experiments were conducted to evaluate the pumping capacity of this pump. A plate made of a 5754 series aluminium alloy, measuring  $12 \times 180 \text{ mm}$ , was inserted between the rows of magnets, and the force applied to the sheet was measured using a hand balance as a function of the rotation frequency of the magnets (Fig. 2.4).

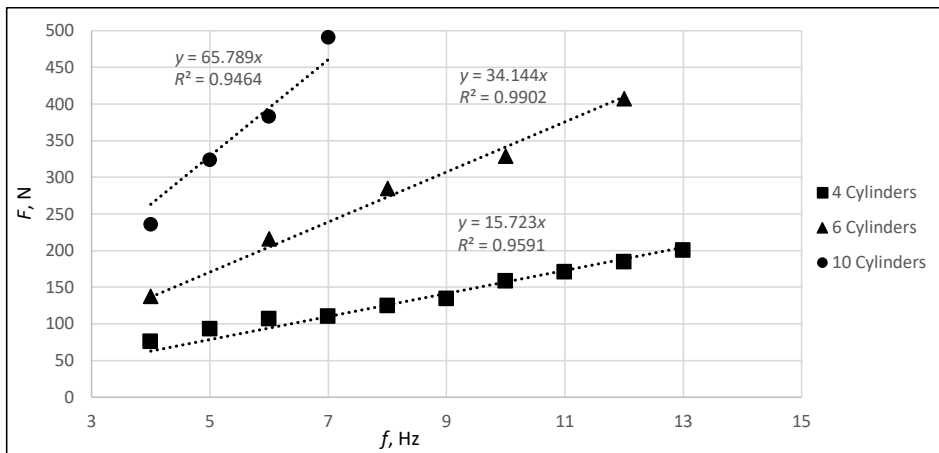


Fig. 2.4. The force exerted by the pump on the aluminium sheet.

In the 4-cylinder configuration used,  $\alpha = 95^\circ$  and  $\beta = 90^\circ$  were set. In the 6- and 10-cylinder configurations,  $\alpha = 95^\circ$  and  $\beta = 180^\circ$  were set. During the experiments, it was observed that the aluminium sheet heated up, and the measured force decreased as a result. This heating effect is caused by joule heat when the magnets induce currents, and its magnitude depends on the rotation frequency. As the rotation speed increases, the heating effect also increases. Moreover, as the temperature of aluminium increases, its conductivity decreases, resulting in a decrease in the electromagnetic force generated. Therefore, it was necessary to wait between measurements when a high speed was used, or if the device was switched on for a long period.

Estimating the pressure such a pump would create in liquid aluminium is possible. A 10-cylinder configuration is considered. The developed pressure is  $p = 227 \text{ kPa}$  at  $7 \text{ Hz}$ . Thus, the height of the pressure column would be

$$h = \frac{F}{S\rho g} = 9.75 \text{ m} \quad (2.12)$$

The study results suggest that a bilateral PM pump with two rotating cylindrical dipole arrays can be practical for specific configurations of magnetisation directions. Optimum phase shift angles for rotor configurations consisting of 4, 6, 8, and 10 magnets were determined.

Analytical calculations showed that the torque minima of the 10 magnets are located at  $\alpha = 49.1^\circ$ ,  $92.8^\circ$ , and  $136.8^\circ$ , which are very close to the numerically calculated values of  $\alpha = 48^\circ$ ,  $93^\circ$ , and  $137^\circ$ . The system was tested experimentally at  $\alpha = 93^\circ$ , which provides the highest value of magnetic induction between the magnets, and it was demonstrated that the system had a stable performance. The difference between the optimal angle  $\alpha$  in the analytical and numerical models could be explained by the magnet end effects, which were not considered in the analytical model, and by the limited finite element mesh size in the numerical model.

Experiments were also conducted with an aluminium plate, demonstrating the high potential of such a pump for liquid metal pumping. However, in real-world applications, there will always be some phase shift error, and therefore, a large number of PM cylinders in such a pump may not be desirable.

### 3. LIQUID METAL MIXERS

#### 3.1. Model experiment for temperature homogenisation of molten metal with a rotating permanent magnet

In metallurgy, handling aluminium poses several challenges due to its high temperature and chemical reactivity in its molten state. Effective mixing is essential for achieving thermal homogenisation and uniform mass composition, which are critical for achieving predictable and uniform crystallization outcomes [6], [7]. Electromagnetic mixing methods have gained popularity due to their non-contact nature, continuous operation, and minimal maintenance requirements, despite being more expensive [6]–[8]. AC inductors are commonly used to generate a shunting or rotating magnetic field, which is necessary to induce fluid flow in electrically conductive fluids. However, the use of AC inductors has been deemed inefficient due to significant power losses in the form of heat caused by the ohmic resistance in the windings [6], [7], [9], [10]. In contrast, permanent magnet systems do not consume energy to generate magnetic fields, making them more energy efficient. The electric motor only consumes energy to rotate the PM block and create motion by overcoming the secondary magnetic fields induced in the liquid metal. Despite this advantage, few studies have been conducted on permanent magnet systems, leaving significant opportunities for developing new applications [11], [12].

The experiment aimed to study the temperature equalisation in a liquid metal volume with a vertical temperature gradient using a rotating permanent magnet. The experimental setup consisted of a stainless-steel container with dimensions of  $0.15\text{ m} \times 0.1\text{ m} \times 0.2\text{ m}$  and a wall thickness of  $0.5\text{ mm}$ . The container was filled with GaInSn eutectic alloy and spray-painted matte black on the outside to increase the emissivity of the wall (shown in Fig. 3.1). The infrared radiation of the container walls was recorded with a thermal camera, and the temperature was calculated assuming black body radiation.

The experimental device included a cylindrical NdFeB permanent magnet with a magnetisation of  $B = 1.42\text{ T}$  and dimensions of  $0.05\text{ m}$  in diameter and  $0.1\text{ m}$  in height. The outer shell of the permanent magnet rotor was made of stainless steel with a thickness of  $2\text{ mm}$ , and the distance between the outer wall of the container and the outer wall of the permanent magnet rotor was  $0.0375\text{ m}$ . Two Type K thermocouples with an accuracy of  $\pm 0.1^\circ\text{C}$  were inserted into the liquid metal to provide reference measurements.

Parametric numerical experiments were also conducted by varying the tilt angle of the magnet to find the most efficient position for thermal equilibrium. The study aimed to identify the most efficient position where thermal equilibrium can be reached the fastest.

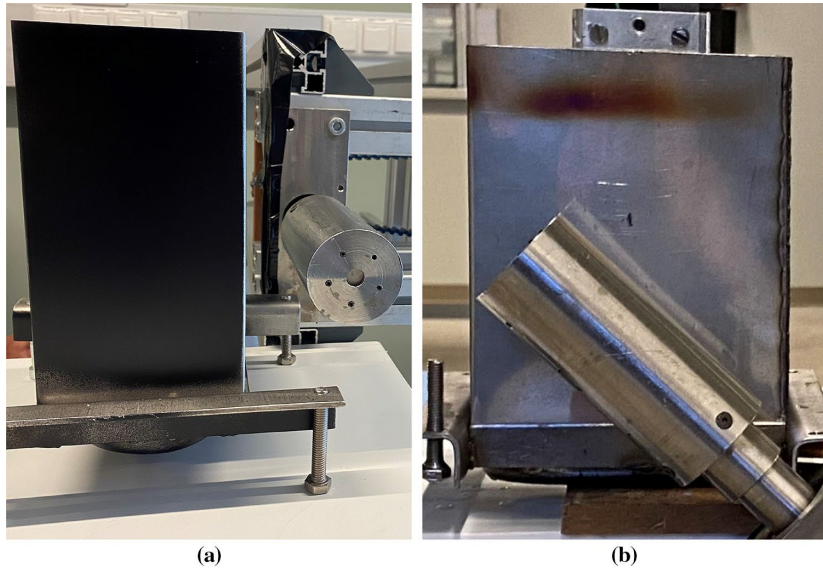


Fig. 3.1. Experimental setup showing the position of the side wall of the black container and the adjacent magnet: (a) horizontal; b) at an inclination angle of 45 degrees.

The GaInSn eutectic alloy was cooled to 22 °C by placing the metal container in cold water to begin the experiment. The top surface of the liquid metal was then heated with a gas burner until the top thermocouple read 82 °C. While heating the upper part of the tank, the temperature in the lower layers of the liquid metal also increased slightly. At the start of the experiment, the lower thermocouple read 24 °C, which may have varied by a few degrees during the experiment.

Next, the permanent magnet rotor was started and an infrared camera (*FLIR T650sc*) with a sensor of  $640 \times 480$  pixels and an accuracy of  $\pm 1$  °C was used to film one side of the container until thermal equilibrium was reached. The experiment was terminated at this point. The permanent magnet was always placed near the widest side of the container, but thermal imaging was performed on both the widest and narrowest sides in successive experiments. As the container wall was made of a thin sheet of stainless steel, the heat transfer was expected to be very fast, and the temperature observed by the thermal imager was assumed to be close to the temperature of the liquid metal behind the wall. The experiment was repeated for different magnet orientations and rotation frequencies, with two frequencies ( $f = 1.1$  Hz and  $f = 7.6$  Hz) and three orientations (vertical, horizontal, and 45°) considered.

The results obtained from both the infrared cameras and thermocouples were compared with the results of the numerical model. The liquid metal temperature readings were taken at two positions – at the top of the tank where the initial temperature was higher and at the bottom where the initial temperature was lower. The temperature changes for each approach were plotted together for all permanent magnet positions and both rotation frequencies, as shown in Fig. 3.2.

Overall, this experiment aimed to investigate the effects of permanent magnet orientation and rotation frequency on liquid metal temperature using both experimental and numerical methods.

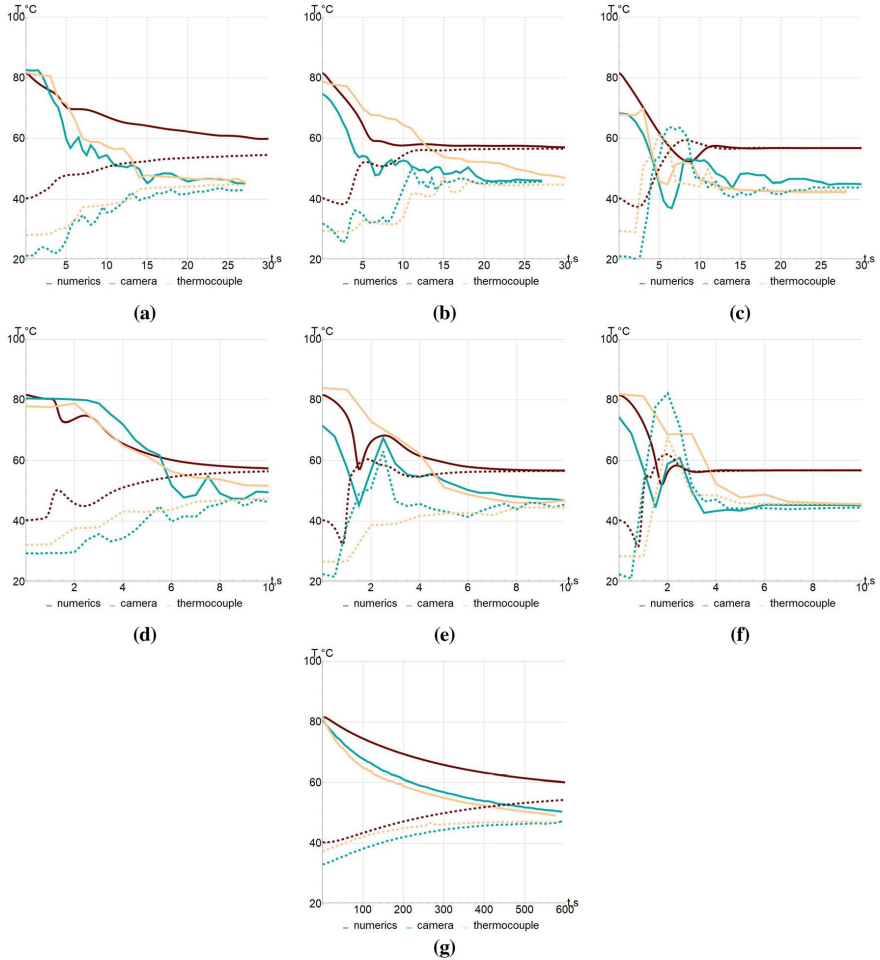


Fig. 3.2. Temperature comparison at rotation frequency 1.1 Hz (a)–(c), 7.6 Hz (d)–(f), and without magnet (g). The upper probe and the lower probe are indicated by solid and dashed lines, respectively. Magnet orientation: (a), (d) vertical; (b), (e) 45 degrees; (c), (f) horizontal.

For a quantitative comparison, the no-stirring case was also included. Additionally, snapshots of the temperature distribution from infrared camera recordings and numerical calculations were used for a qualitative comparison between the experiment and the numerical model, as shown in Fig. 3.3.

As the rotation frequency of the permanent magnet increased, the mixing of the hot and cold liquid metal regions accelerated. To better visualise the mixing process and convection patterns, the results of the 1.1 Hz experiments were used for the qualitative comparison.

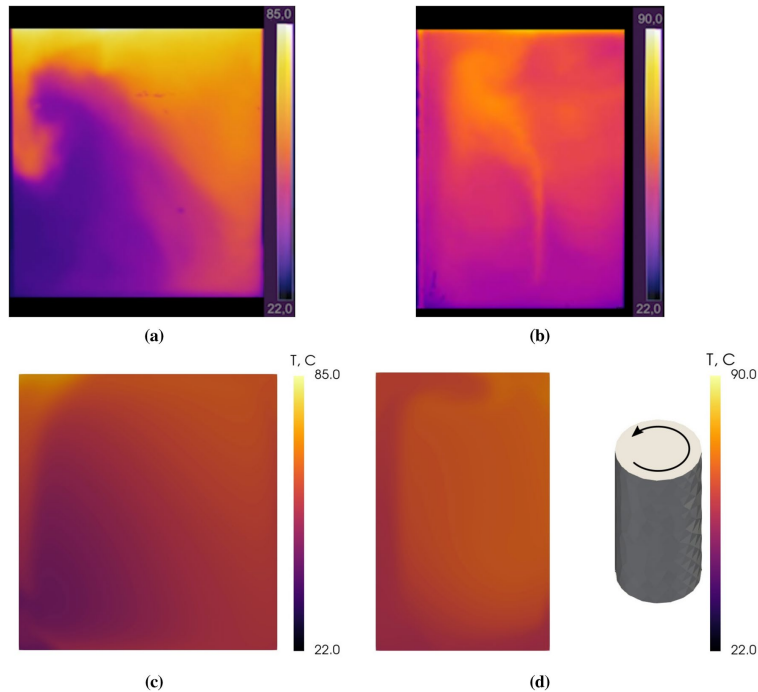


Fig. 3.3. Temperature distribution of the side wall in the physical experiment and numerical calculation at the PM rotation frequency of 1.1 Hz, when the magnet is placed at an angle of 45 degrees: (a) physical experiment – wider side; (b) physical experiment – the narrower side; (c) numerical calculation – wider side; (d) numerical calculation – the narrower side.

Although the results of the numerical calculations are not in perfect agreement with the experimental data, they generally agree well, given the limitations of the numerical model. The most significant discrepancy between the two is seen in the initial and final temperatures. In all cases, the numerical calculation reading of the lower probe starts slightly higher. This can be attributed to the initial linear temperature distribution assumed in the numerical model. The heat from the gas burner had not yet reached the bottom depth of the probe at the beginning of the experiment, leaving the bottom layers at room temperature. Furthermore, the numerical model assumes adiabatic wall boundary conditions for temperature, whereas the experiment involves heat loss from the container walls, affecting the liquid metal's final temperature. Despite these discrepancies, the observed temperature homogenisation process is not significantly affected.

The experimental model successfully demonstrates that thin-walled stainless steel containers, in combination with a thermal imaging camera, can be used to observe the flow of liquid metal at different temperatures. The rotating permanent magnet dramatically improves the

time required to reach thermodynamic equilibrium in a volume of liquid metal. The experimental results show that the best way to mix a liquid metal that has a vertical temperature gradient is by placing the rotating permanent magnet in a horizontal position. These results suggest that the single dipole permanent magnet stirrer is an effective solution for achieving thermal equilibrium in top-heated metal melting furnaces.

In future research, direct temperature measurements could be improved by replacing the thermocouples in the enclosures with thin thermocouple wires placed directly on the container wall. This should improve the agreement between different measurement methods. Additionally, the numerical model can be further developed and scaled to an industrial-sized model.

### 3.2. Two-cylinder mixer

In gas burner-powered metal melting furnaces, it is crucial to mix the liquid metal thoroughly. Failing to do so leads to a significant temperature disparity between the top and bottom layers of the metal, typically ranging from 50 °C to 80 °C [13]. High surface temperatures also encourage oxidation and scale formation. Effective bulk mixing of liquid metal is essential for metal fabricators, as it enables faster mixing of alloying materials and promotes uniformity in both chemical composition and temperature. Liquid metal mixers are useful for mixing, degassing, and manipulating the crystallisation structure of alloying materials.

The two-cylinder mixer was developed to explore liquid metal flow in cylindrical vessels when two permanent magnets are placed on either side. The device is depicted in Fig. 3.4. Its primary functions include investigating effective methods for liquid metal mixing and particle mixing.

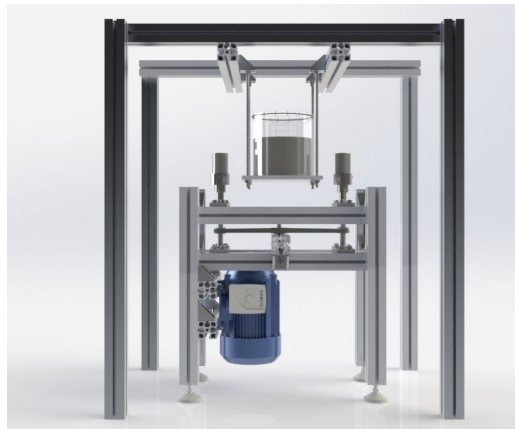


Fig. 3.4. Image of a computer model of the experimental setup.

The system comprises two primary structures. The central equipment consists of two cylindrical permanent magnets (PMs) with parallel axes of rotation. The magnets are housed in stainless steel frames affixed to cylindrical axes connected to a Siemens three-phase motor with a power output of 0.55 kW and a maximum speed of 1440 rpm, using toothed belts and rollers. Two tensioning rollers ensure proper belt tension at all possible distances between the PMs, while also

facilitating mutual rotation of the magnets in either the same or opposite directions. To minimise the transfer of vibrations, the frame holding the liquid metal container is separated from the PM frame.

Furthermore, the frame containing the magnets can be tilted in relation to the container holding the liquid metal using specialised fasteners. The angle of inclination between the magnets and the ground is represented by  $\theta$ , while the initial magnetisation direction of the magnets in relation to each other is denoted by  $\varphi$ . The liquid metal container has a volume of  $V = 1.7$  L and dimensions of 130 mm in diameter and 134 mm in height.

During velocity measurements, it was observed that the phase shift angle  $\varphi = 0^\circ$  in co-rotation modes resulted in the highest flow velocities, which were approximately 5–10 % greater than those observed at  $\varphi = 90^\circ$  or  $\varphi = 180^\circ$ . No significant difference was noted in anti-rotation modes. The effect of different phase shifts is minimal in this case, as the magnets are relatively distant. Figure 3.5 illustrates the measured flow rates versus magnet rotation speed at various phase shifts  $\varphi$ , when  $\theta = 90^\circ$ .

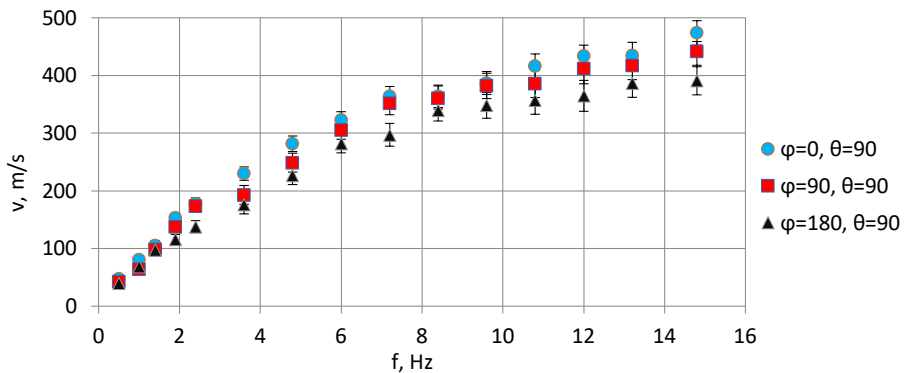


Fig. 3.5. Flow speed relative to magnet rotation speed (co-rotation).

An experimental device was used to demonstrate that the PM system can generate intense motion within a volume of liquid metal. The equipment's versatility allowed various flow types to be achieved in a cylindrical vessel. Dimensionless analysis was conducted, indicating that the system can mix large volumes of liquid aluminium in industrial processes. The magnetic field was measured experimentally, and the results agreed with those obtained from a numerical model, demonstrating the suitability of *COMSOL Multiphysics* for calculating the magnetic field of PM systems.

This technology has several advantages, such as its simplicity and energy efficiency. However, it also has some limitations, such as a constant magnetic field and limited applicability in the case of thick walls.

## 4. CONCLUSIONS

1. It has been experimentally shown that a single permanent magnet cylinder can efficiently pump liquid metal when placed near a wide channel with a small height. The induced current loops, acting on the primary magnetic field, create a force on the liquid metal, resulting in a pressure difference of 14 kPa at a magnet rotation frequency of 71 Hz. It was found that the currents induced as a result of permanent magnet rotation produce 73 % of heat power, which corresponds to 21 % of the motor power.
2. It is concluded that scaling up small-scale experimental liquid metal pumps to larger-scale industrial equipment can be achieved by analysing dimensionless quantities.
3. The observed recirculating flow caused by a single PM pump in a liquid metal channel is associated with side wall effects.
4. A methodology for calculating the mutual forces of cylindrical PM dipoles has been developed, and an analytical, numerical, and experimental study of systems with several PM cylinders in two rows has been implemented.
5. Optimization of the engine torque was carried out by changing the magnetisation directions of the PM. It was found that for PM systems with closely spaced PM dipoles, there exists an optimal phase shift angle of the mutual magnetisation directions in relation to the average torque of the system. In a system with 6 cylinders, the optimal angle  $\alpha = 97^\circ$ ; in a system with 8 cylinders, the optimal angle  $\alpha = 78^\circ$ ; and in a system with 10 cylinders, the optimal angle  $\alpha = 48^\circ$ ,  $\alpha = 93^\circ$ , and  $\alpha = 137^\circ$ .
6. Numerical and analytical calculations show that, to develop a device with several cylinders of permanent magnets capable of stable operation, it is necessary to set specific phase angles of magnetisation directions. Even small deviations from these optimum angles can cause heavy loads on the drive system.
7. A single PM cylinder device was developed to study degassing processes. Analytical and numerical calculations show that this design can generate sufficient liquid aluminium flow in the chamber to perform degassing and break gas bubbles. It has been found that, with the help of ferromagnetic yokes, a 20 % stronger magnetic field can be obtained in the liquid metal zone.
8. It was concluded that a single dipole permanent magnet stirrer is an effective solution for achieving thermal equilibrium in metal melting furnaces heated from above, and a horizontally placed magnet stirs the liquid at least 2 times faster.
9. A 2 PM cylinder liquid metal stirring device was developed and demonstrated that it can create intense motion in a volume of liquid metal. Different types of flow in a cylindrical vessel were realised, and it was demonstrated that the two PM cylinder system can be successfully used for liquid metal mixing. It has been found that the highest speeds are achieved at the mutual magnetisation phase shift angle  $\varphi = 0^\circ$ , up to 0.47 m/s at the magnet rotation frequency of 19.2 Hz.

## BIBLIOGRAPHY

- [1] A. Bojarevics and T. Beinerts, “Experiments on liquid metal flow induced by a rotating magnetic dipole,” *Magneto hydrodynamics*, vol. 46, no. 4, pp. 333–338, 2010.
- [2] L. Zhang, X. Lv, A. T. Torgerson, and M. Long, “Removal of Impurity Elements from Molten Aluminum: A Review,” <http://dx.doi.org/10.1080/08827508.2010.483396>, vol. 32, no. 3, pp. 150–228, Jul. 2011, doi: 10.1080/08827508.2010.483396.
- [3] D. E. J. Talbot, “Effects of Hydrogen in Aluminium, Magnesium, Copper, and Their Alloys,” <https://doi.org/10.1179/imtlr.1975.20.1.166>, vol. 20, no. 1, pp. 166–184, Jan. 2013, doi: 10.1179/IMTLR.1975.20.1.166.
- [4] G. K. Sigworth, E. M. Williams, and D. C. Chesonis, “Gas fluxing of molten aluminum: An overview,” *TMS Light Metals*, pp. 581–586, 2008, doi: 10.1007/978-3-319-48228-6\_9.
- [5] K. Halbach, “Design of permanent multipole magnets with oriented rare earth cobalt material,” *Nuclear Instruments and Methods*, vol. 169, no. 1, pp. 1–10, Feb. 1980, doi: 10.1016/0029-554X(80)90094-4.
- [6] Cook, R., Varayud, M., Iijima, S., & Takahashi, E., “Case Study of Magnetically-Stirred Casting Furnaces at New Zealand Aluminium Smelters Limited,” in *Light Metals 2017*, A. P. Ratvik, Ed., Cham: Springer International Publishing, 2017, pp. 909–915.
- [7] J. Herbert and B. Painter, “Case Study of Air Cooled Electromagnetic Stirred Melting Furnace at Hydro Henderson,” in *TMS Annual Meeting & Exhibition*, Springer, 2018, pp. 1015–1023.
- [8] A. Peel and P. Y. Menet, “The application of MHD side stirring technology to aluminium melting furnaces for operational efficiency improvement – a case study,” *Journal for Manufacturing Science and Production*, vol. 15, no. 1, pp. 59–67, 2015.
- [9] A. Bojarevičs, R. Baranovskis, I. Kaldre, M. Milgrāvis, and T. Beinerts, “Two cylinder permanent magnet stirrer for liquid metals,” in *IOP Conference Series: Materials Science and Engineering*, IOP Publishing, 2017, p. 012022.
- [10] J. Zeng, W. Chen, Y. Yang, and A. Mclean, “A review of permanent magnet stirring during metal solidification,” *Metallurgical and materials transactions B*, vol. 48, no. 6, pp. 3083–3100, 2017.
- [11] I. Buceniaks, “Perspectives of increasing efficiency and productivity of electromagnetic induction pumps for mercury basing on permanent magnets,” in *International Conference on Nuclear Engineering*, 2006, pp. 185–189.
- [12] I. Kaldre *et al.*, “Contactless electromagnetic method for aluminium degassing,” in *IOP Conference Series: Materials Science and Engineering*, 2018. doi: 10.1088/1757-899X/424/1/012057.
- [13] J. Andersson, “Optimized Electromagnetic Stirring in Melting and Holding Furnaces BT – Light Metals 2019,” C. Chesonis, Ed., Cham: Springer International Publishing, 2019, pp. 1179–1183.



---

**Matīss Kalvāns** was born in 1989 in Riga. He obtained a Bachelor's degree in Physics from the Université Pierre-et-Marie-Curie (Paris, France) in 2012 and a Master's degree in Mechanical Engineering from the University of Glasgow (Glasgow, Great Britain) in 2014. He has been a researcher with the Institute of Physics of the University of Latvia since 2014. His scientific interests are related to permanent magnets, metallurgy, and magnetohydrodynamics.